J. Membrane Biol. 15, 67–86 (1974)

Computer Simulation of the Response of Frog Skin Epidermis to Changes in $[Na^+]_0$

Ernst G. Huf and John R. Howell

Departments of Physiology and Biometry, Virginia Commonwealth University, Richmond, Virginia 23219

Received 8 June 1973; revised 27 September 1973

Summary. The operation of the multicompartmental frog skin epidermal model 10E described in the preceding paper was tested to find out by computer simulation whether it responds to changes in $[Na^+]$ in the same manner as frog skin. In the range from 5 to 115 mM $[Na^+]_0$, the rate of net Na^+ flux across skin is known to increase. The results can be fitted to Michaelis-Menten's law of reaction kinetics, or, alternately, to Hoshiko's linear function, plotting flux *vs.* log $[Na^+]_0$. Model 10E simulated the laboratory results on skin, provided that the rate coefficients at the site of entry of Na^+ into the system were varied in exactly the same manner as they actually were found to vary in skin. In model studies, Na^+ backflux (outflux) decreased with increasing $[Na^+]_0$, contrary to observations on skin. This discrepancy may be related to adaptive reactions in skins (decrease in permeability) when $[Na^+]_0$ is lowered, a feature that has not been modeled. It is known that the skin p.d. changes, mostly, by approximately 35 mV per decade change in $[Na^+]_0$. Model 10E gave very nearly the same result when the rate coefficients for entry of Na^+ were changed as mentioned above (i.e., varied exactly as they were found to vary in skin). Skin and model 10E behaved similarly in that, at $[Na^+]_0 = [Na^+]_i = 115$ mM, the extent to which labeling with Na* from the outside (12%) and from the inside (88%) is possible was the same. Model data are presented which show in which way the Na^+ pools, $[Na^+]$ in the individual compartments, and intercompartmental fluxes changed with changing $[Na^+]_0$. Because of lack of experimental data on skin for comparison, these calculated results are purely hypothetical, but they are not unreasonable.

When isolated frog skin is mounted between two oxygenated frog Ringer's solutions, one observes a net transport of NaCl in the direction from the epidermis to the corium [9]. This results from an active inward transport of Na^+, with Cl^- following passively [23]. The rate of net Na^+ transport (J_n^{Na}) is approximately 1 $\mu Equiv \times cm^{-2} \times hr^{-1}$. When the $[Na^+]$ on the epidermal side (outside) is lowered, the rate of active inward Na^+ transport and of J_n^{Na} is found decreased [3, 22]. A plot of J_n^{Na} *vs.* $[Na^+]_0$ suggests saturation kinetics of the active Na^+ transport process. The

electrical skin potential changes, ideally, by 58 mV per decade change in $[Na^+]_0$ [14]. More often, however, the skin potential changes by less than 58 mV; a value of approximately 35 mV has been reported by several investigators [2, 7, 15–17, 21].

The difficulties in interpreting these findings from the standpoint of epidermal structural-functional relationships arise from the fact that the skin is a rather complex multicompartmental organ. Neither the location of the active Na^+ transport mechanism (the Na^+ pump) nor the pathways that ions travel across the skin are clearly established. Consequently, all efforts to describe the kinetics of ion flows across the skin must remain speculative until the functional significance of the many structural components is no longer in doubt. The simplest hypothesis is to assume that all but one compartment in the epidermis, the Na^+ transport compartment, need be considered [5]. Along this line several interesting studies have been published [2–4, 6, 18, 19], although even with this oversimplified assumption, no clear evidence has been provided as to the location of this Na^+ transport compartment within the multilayered epidermis. Another hypothetical approach for kinetic analysis is to design a more realistic model, based on histological and experimental facts. There are at least four distinct but interconnected compartments within the epidermis: 1) the subcorneal space; 2) the "first reacting cell layer" (1. RCL); 3) the remaining epithelial cells; and 4) the extracellular space (*see* preceding paper for references). Since direct experimental measurements on Na^+ flows in and across such an epidermal multicompartmental system, for the present, are beyond approach, we have recently attempted to gain detailed information on the operation of such a system by computer simulation. The operation of the model, designated earlier [10] as model 10E, simulated to a remarkable degree the facts as we know them from studying Na^+ transport in frog skin.

It was the aim of the present study to use this same model 10E to simulate the response of frog skin to changes in $[Na^+]_0$, both in regard to changes in transepithelial Na^+ flux rates and to changes in electrical skin potential. By doing this we were again able to obtain detailed information on the operation of the model, and especially to observe the associated changes in individual Na^+ pools, and the $[Na^+]$ in the various compartments for steady-state conditions.

1. The Model 10E

The basic model used in this study is in all respects identical to model 10E described earlier [10]. Compartments 1 and 7 in Fig. 1 of the preceding

paper [10] correspond to "outside" (o), and "inside" (i) solution in skin experiments. Subscripts 1 (o) and 7 (i) are used interchangeably in the following text and illustrations.

2. The Models 22 through 32

In the eleven models designated by numbers 22 through 32 only the initial conditions and the k_{13} and k_{31} values differed from those used in 10E. In *influx studies* the S_1 values chosen were: $S_1 = 25$ (model 22); 57.5 (23); 100 (24); 150 (25); 200 (26); 250 (27); 300 (28); 350 (29); 400 (30); 450 (31); and 500 (32). This is equivalent to varying $[Na^+]_1$ from 5 mM (22) to 100 mM (32). All other S_j's $= 0$ at $t = 0$. In *outflux studies*, $S_7 = 575$ ($[Na^+]_7 = 115$ mM); all other S_j's $= 0$ at $t = 0$. In *net flux studies*, S_1 was varied as stated above, and $S_7 = 575$. *Rate constants* (min^{-1}): $k_{13} = 0.000152$, $k_{31} = 0.49$ (model 22); $k_{13} = 0.000126$, $k_{31} = 0.46$ (23); $k_{13} = 0.000098$, $k_{31} = 0.436$ (24); $k_{13} = 0.000076$, $k_{31} = 0.40$ (25); $k_{13} = 0.000060$; $k_{31} = 0.368$ (26); $k_{13} = 0.000048$; $k_{31} = 0.34$ (27); $k_{13} = 0.000038$; $k_{31} = 0.314$ (28); $k_{13} = 0.000032$; $k_{31} = 0.286$ (29); $k_{13} = 0.000026$; $k_{31} = 0.264$ (30); $k_{13} = 0.000024$; $k_{31} = 0.24$ (31); $k_{13} = 0.000022$; $k_{31} = 0.222$ (32). The reason for choosing these values will be given in Section 5*a*.

3. Flow Equations and Solutions

The six simultaneous linear differential flow equations describing the operation of the models, both in conventional and matrix form are given in the preceding paper [10]. Estimations for the amounts of Na^+ in the compartments (S-values) were obtained by the use of an IBM 360 computer with application of the Continuous System Modeling Program (CSMP). The integration interval was 0.01 min. Print-out data were collected for 30 min at 0.2-min intervals, which was in all cases sufficient to achieve steady-state conditions. The data were printed out in 5, and in some cases in 7 decimals when the absolute values of S_j were small. A computational error analysis is presented in the Appendix.

4. Calculations

Transmembrane Steady-State Na^+ *Flux Rates*

These were calculated in two ways with nearly identical results, the difference in results amounting to no more than 1%. (a) Calculations by

directly using the difference of the 30-min and the 25-min print-out numbers. (b) Calculations by using the integrated steady-state flux Eqs. (8) and (9) given in the preceding paper [10]. Flux rates are given as μEquiv × cm^{-2} × hr^{-1}.

Steady-State Flux Rates for Na^+ *Between Individual Compartments*

These were obtained by applying the equation $J = k \times S$, using the appropriate k and steady-state S values, e.g., $J_{12} = k_{12} \cdot S_1$. Then $(J_{12} - J_{21})$ is the net flux between compartments.

Steady-State $[Na^+]$ *in the Individual Compartments*

This was calculated as S_j/V_j, where S_j is the print-out number read at $t = 30$ min, taken as μEquiv Na^+ in compartment j, and V_j is the corresponding compartmental colume (*see* model 10E), assumed to remain constant.

Na^+ *Pool Fraction of the Individual Compartments*

This was calculated as S_{ji}/S_{jn}, where S_{ji} is the 30-min steady-state print-out number in compartment j under influx initial conditions, and S_{jn} is the print-out number under net flux initial conditions.

Total Na^+ *Pool Fraction;* V_{23}

Similarly, a value for $\Sigma S_{2i} S_{3i} S_{4i} S_{5i} / \Sigma S_{2n} S_{3n} S_{4n} S_{5n}$ was calculated. For calculation of the electrical potential difference between compartments 2 and 3 (subcorneal space/1. RCL) the equation $V_{23} = 58 \log [Na^+]_2/[Na^+]_3$ was used. The assumption is made that, as postulated by Koefoed-Johnson and Ussing [14], the outward facing membrane of the 1. RCL behaves like a Na^+ permselective membrane.

5. Results

(a) Choosing Rate Constants for Entry of Na^+

The experimental data underlying this study are those of Ussing [22], Cereijido, Herrera, Flanigan and Curran [3] and Koefoed-Johnson and Ussing [14]. At the site of entry of Na^+ into the Na^+ transport compartment (Cereijido *et al.*'s compartment No. 2), both k_{21} and, more so k_{12}, decreased with increasing $[Na^+]_0$. Because these data are most essential for the present

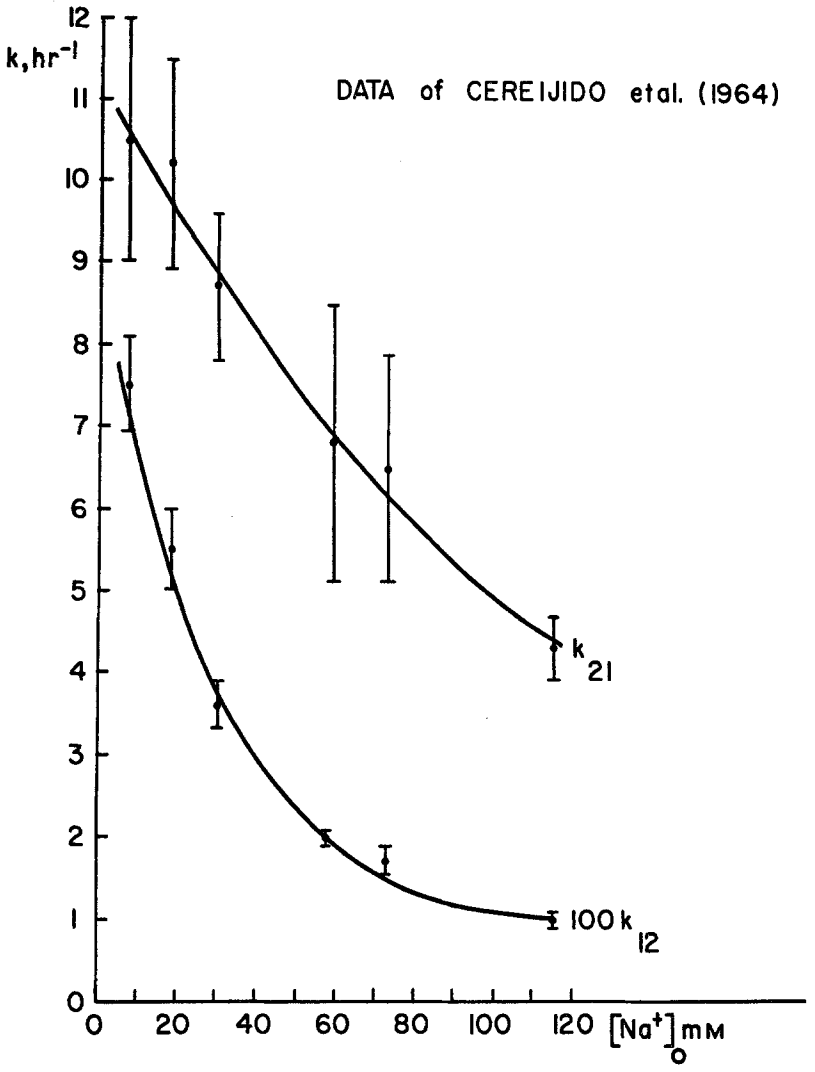

Fig. 1. Dependence of rate coefficients k for entry of Na^+ on $[Na^+]_0$, i.e. $[Na^+]$ at the epidermal side of the skin. k_{12} and k_{21} are the rate coefficients at the outer border in Cereijido *et al.*'s three-compartment model [3, 5]

work, the results given in their Table 1 are plotted in Fig. 1. The curves are drawn by eye. From these graphs we have calculated by what factors k_{12} and k_{21} change when $[Na^+]_0$ is varied from 5 to 115 mM, assigning to the k_{12} and k_{21} at 115 mM a relative value of 1.0. Such factors were calculated for $[Na^+]_1$ varying in the steps given in Section 2. It should be noted that by applying these factors to model 10E, experimentally established numbers, not arbitrary ones, were put to use. The k_{21} values are afflicted with a

Table 1. Steady-state changes in electrical potential (ΔV_{23}), and net Na^+ flux values (J_n^{Na}) resulting from decreasing $[Na^+]_1$ from 115 to 11.5 mM[a]

	Model 19[b] changing only k_{12}, k_{21}	Model 23 changing only k_{13}, k_{31}	Model 21 changing k_{12}, k_{21} and k_{13}, k_{31}
k_{12}	0.00101[c]	0.00016 } Model 10E	0.00101
k_{21}	18.4[d]	8.0 }	18.4
k_{13}	0.00002 } Model 10E	0.000126	0.000126
k_{31}	0.2 }	0.46	0.46
$[Na^+]_2$	29.99	10.50	29.96
$[Na^+]_3$	2.14	2.87	3.26
V_{23}	66.5	32.7	55.9
ΔV_{23}	−6.7[e]	−40.6	−17.4
J_n^{Na} 1 → 7	0.22	0.43	0.54

[a] $[Na^+]_7 = 115$ mM. k-values not listed in the table are given in the text for 10E, section 1.
[b] k's in min^{-1}; $[Na^+]$ in mM; V in mV; J_n^{Na} in μEquiv × cm^{-2} × hr^{-1}.
[c] $0.00016 \times 6.3 = 0.00101$.
[d] $8.0 \times 2.30 = 18.4$, where the factors are obtained from Fig. 1 as explained in the text, Section 5*a*.
[e] V_{23} for the case $[Na^+]_1 = [Na^+]_7 = 115$ mM is 73.3 mV; $V_{23} = 58 \log [Na^+]_2/[Na^+]_3$.

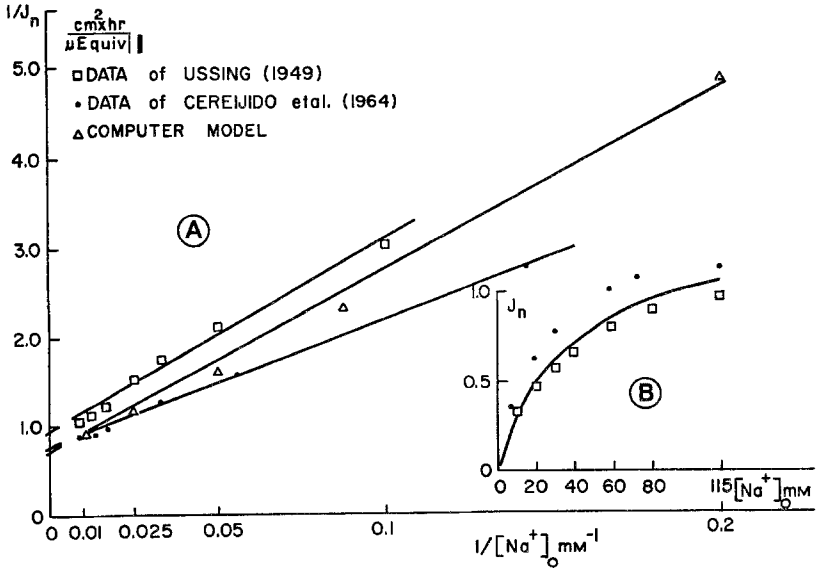

Fig. 2. Dependence of steady-state net Na^+ flux on $[Na^+]_0$. (*A*) Double reciprocal plot. (*B*) J_n^{Na} *vs.* $[Na^+]_0$. Solid line = plot of Eq. (7). □ and •, experimental data as quoted in *A*

considerable SEM, but these data are the only ones that are presently available. What is arbitrary, however, is that we have applied the factors to pathway $1 \leftrightarrow 3$, and not to $1 \leftrightarrow 2$ in model 10E shown in Fig. 1 of ref [10]; e.g. according to Cereijido *et al.* [3] at $[Na^+]_0 = 50$ mM, k_{12} was $2.4 \times k_{12}$ for $[Na^+]_1 = 115$ mM; and k_{21} was $1.70 \times k_{21}$ for $[Na^+]_1 = 115$ mM. These factors, when applied to model 10E, pathway $1 \leftrightarrow 3$, give for $k_{13} = 0.000048$ and for $k_{31} = 0.34$. The changes in rate constants for pathway $1 \leftrightarrow 3$, with changes in $[Na^+]_1$ given in Section 2 were obtained in this manner. The reason why the pathway $1 \leftrightarrow 2$ was not considered altered is given by the data in Table 1. Here, results are shown which were obtained when altering pathway $1 \leftrightarrow 2$ only; or $1 \leftrightarrow 3$ only; or both $1 \leftrightarrow 2$ and $1 \leftrightarrow 3$. Referring to skin, the experimental facts are that when $[Na^+]_0 = 11.5$ mM and $[Na^+]_i = 115$ mM, the net flux of Na^+ is close to 0.4 μEquiv × cm^{-2} × hr^{-1} (*see* Fig. 2*B*), and the open skin potential increases by approximately 35 mV. These results are best simulated by changing k_{13} and k_{31}. We have proceeded, therefore, under the assumption that by varying $[Na^+]_1$, the pathway $1 \leftrightarrow 3$, i.e., the rate of flow of Na^+ via the cornified layer and the cell junctions into or out of the 1. RCL, is primarily affected. The computer runs on models 19 and 21 (Table 1) showed that during steady state $[Na^+]_2 > [Na^+]_1$ with continuing net inward Na^+ flux. It seemed to us that a concentration profile as seen in model 23 merits preferred attention.

(b) Dependence of Na^+ *Flux on* $[Na^+]_1$ (*"outside"* $[Na^+]_0$). *Net Flux*

By varying $[Na^+]_1$ from 5 to 115 mM and by applying the appropriate changes to the k_{13} and k_{31} values as explained in Section 5*a*, data were obtained from which the rates for influx, backflux and net Na^+ flux were calculated. We report here only the results on net flux and backflux. From this the influx rates can be calculated, if desired, using Table 2.

Table 2. Dependence of steady-state Na^+ backflux (J_b^{Na}) on $[Na^+]_1$[a]

Model No.	22	23	24	25	26	27
$[Na^+]_1$, mM	5	11.5	20	30	40	50
J_b^{Na}, μEquiv/(cm^2 × hr)	0.026	0.025	0.024	0.023	0.021	0.021
J_b^{Na} in % J_i^{Na}	11.0	5.4	3.7	2.9	2.4	2.2
Model No.	28	29	30	31	32	10E
$[Na^+]_1$, mM	60	70	80	90	100	115
J_b^{Na}, μEquiv/(cm^2 × hr)	0.020	0.018	0.018	0.017	0.016	0.015
J_b^{Na} in % J_i^{Na}	2.1	1.8	1.8	1.6	1.4	1.2

[a] $[Na^+]_7$ in all cases 115 mM. Values for J_i^{Na} and J_b^{Na} were rounded out to 3 decimals.

Net Flux. Figs. 2 and 3 show the results on changes in net flux. In Fig. 2*A* the double reciprocal plot of $1/J_n^{Na}$ *vs.* $1/[Na^+]_0$ was chosen to show the dependency of flux on $[Na^+]_0$. Actual laboratory results published by Ussing [22], and by Cereijido *et al.* [3] are compared with results obtained by computer simulation. The calculated linear regression equations are as follows:

Data of Ussing:

$$\frac{1}{J_n^{Na}} = 0.92 + 21.95 \frac{1}{[Na^+]_0}; \quad r = 0.992. \tag{1}$$

Data of Cereijido *et al.*:

$$\frac{1}{J_n^{Na}} = 0.76 + 14.20 \frac{1}{[Na^+]_0}; \quad r = 0.999. \tag{2}$$

Data by computer simulation:

$$\frac{1}{J_n^{Na}} = 0.68 + 20.44 \frac{1}{[Na^+]_0}; \quad r = 0.998. \tag{3}$$

These equations may formally be looked upon as Lineweaver-Burke plots of the Michaelis-Menten equation

$$\frac{1}{J_n^{Na}} = \frac{1}{J_{max}^{Na}} + \frac{K_m}{J_{max}^{Na}} \cdot \frac{1}{[Na^+]_0}. \tag{4}$$

Rearranging Eqs. (1), (2) and (3) yields

$$J_n^{Na} = 1.067 \frac{[Na^+]_0}{23.34 + [Na^+]_0} \quad \text{(Ussing)} \tag{5}$$

$$J_n^{Na} = 1.280 \frac{[Na^+]_0}{18.01 + [Na^+]_0} \quad \text{(Cereijido } et\ al.\text{)} \tag{6}$$

and

$$J_n = 1.391 \frac{[Na^+]_0}{38.00 + [Na^+]_0} \quad \text{(computer models)} \tag{7}$$

where the numbers in front of the fractional term are the J_{max}^{Na} values, and the numbers in the denominator are the apparent Michaelis-Menten constants. Eq. (7) is plotted in Fig. 2*B* (solid line). Also shown are the actual

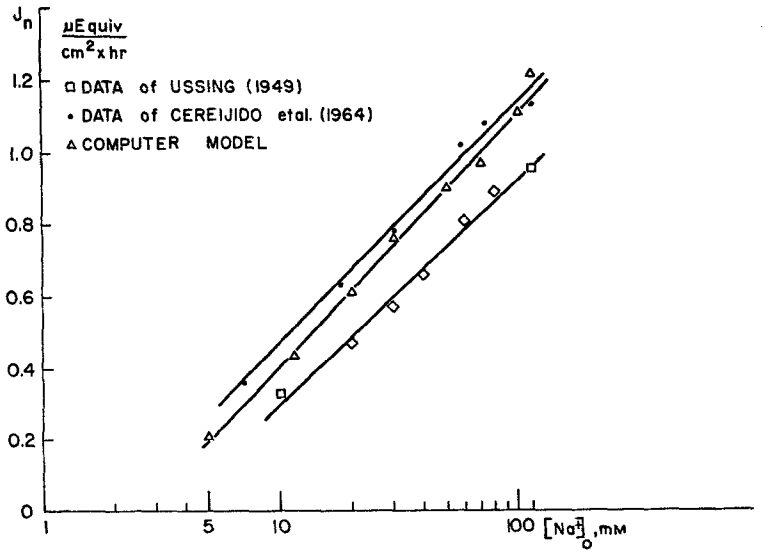

Fig. 3. Dependence of steady-state net Na^+ flux on $[Na^+]_0$. J_n^{Na} is plotted against $\log [Na^+]_0$

results obtained by Ussing [22], and by Cereijido *et al.* [3]. As can be seen from Fig. 2*A* and 2*B*, model 10E, with appropriate changes in k_{13} and k_{31} to give models 22 through 32, describes reasonably well the dependence of net Na^+ flux ($1 \rightarrow 7$) on $[Na^+]_0$. It should be mentioned that the experimental conditions chosen by Ussing and by Cereijido *et al.* were not the same. Ussing measured fluxes across the electrically "open" skin, and he increased $[Na^+]_0$ by adding NaCl in substance. From his influx and outflux data, we have calculated net flux rates. Cereijido *et al.* used short-circuited skins and replaced NaCl on both sides in certain steps by choline chloride. Nevertheless, the results from both laboratories are quite similar.

The dependence of net Na^+ flux on $\log [Na^+]_0$ is shown in Fig. 3 from which it again seems that model 10E responds to changes in $[Na^+]_0$ very similar to the way in which frog skin epidermis responds. This plot is based on considerations by Hoshiko [8]:

$$I_s = gE = 58\, g \log \left(\frac{[K^+]_c}{[Na^+]_c [K^+]_i} \right) + 58\, g \log [Na^+]_0 \tag{8}$$

where I_s is the short-circuit current (net Na^+ flux in skin between Ringer's solution), and g is the skin conductance. Since $[K^+]_c$ increases with increasing $[Na^+]_c$, although not in a simple stoichiometric relationship [11],

the fraction term in the equation may well remain fairly constant; and if one concurs with Hoshiko's assumption that g remains constant, the net Na^+ flux should be a linear function of $[Na^+]_0$. At any rate, when the net flux data of Ussing [22], and Cereijido *et al.* [3], as well as those of models 10E and 22 through 32 were plotted in this way, the graphs shown in Fig. 3 were obtained. The linear regression equations ($r = 0.994$) for these relationships are:

$$J_n^{Na} = -0.32 + 0.62 \log [Na^+]_0 \quad \text{(Ussing)} \tag{9}$$

$$J_n^{Na} = -0.20 + 0.67 \log [Na^+]_0 \quad \text{(Cereijido } et\ al.\text{)} \tag{10}$$

$$J_n^{Na} = -0.29 + 0.70 \log [Na^+]_0 \quad \text{(computer models).} \tag{11}$$

Backflux. The rate of steady-state Na^+ backflux (J_b^{Na}) decreased with increasing $[Na^+]_1$ (Table 2). Net loss from compartment 7 was nearly the same as net gain in compartment 1, adding what enters from $2 \rightarrow 1$ and from $3 \rightarrow 1$. The difference in the two results did not exceed 2.3% (10E). Net loss from 7 slightly exceeded the gain in 1. We attribute this, mainly, to errors in computing. Ussing [22] and Kirschner [13] found that Na^+ outflux (backflux) increases with increasing outside $[Na^+]_0$. A possible reason for this discrepancy will be discussed in Section 6.

(c) Changes in Compartmental $[Na^+]$

From the steady-state Na^+ pool sizes in compartments 2, 3, 4 and 5 under net flux conditions, values for the $[Na^+]$ in these compartments were calculated as explained in Section 4. $[Na^+]_7$ was 115 mM in all cases, but $[Na^+]_1$ varied from 5 mM (model 22) to 115 mM (model 10E). The results are shown in Fig. 4. $[Na^+]_2$, $[Na^+]_3$ and $[Na^+]_4$ slightly increased with increasing $[Na^+]_0$. In all cases $[Na^+]_3$ (1. RCL) $\ll [Na^+]_4$ (remaining epithelial cells). $[Na^+]_5 > 115$ mM, i.e. the solution in compartment 5 (extracellular space) was hypertonic with respect to the "inside solution" in compartment 7. For $[Na^+]_0 = 5$ mM, $[Na^+]_5 = 116.72$ mM; for $[Na^+]_0 = 115$ mM, $[Na^+]_5 = 125.37$ mM. $[Na^+]_2$ rose sharply with increasing $[Na^+]_0$. However, $[Na^+]_2$ (and $[Na^+]_3$) remained always below $[Na^+]_0$. The dashed line in Fig. 4 shows how $[Na^+]_2$ would have to change to attain $[Na^+]_2 = [Na^+]_0$.

(d) Changes in Electrical Potential (V_{23})

For $[Na^+]_1 = 11.5$ mM, $[Na^+]_2$, and $[Na^+]_3$ were 10.50 and 2.87 mM, respectively. For $[Na^+]_1 = 115$ mM, $[Na^+]_2$ and $[Na^+]_3$ were 102.73 and

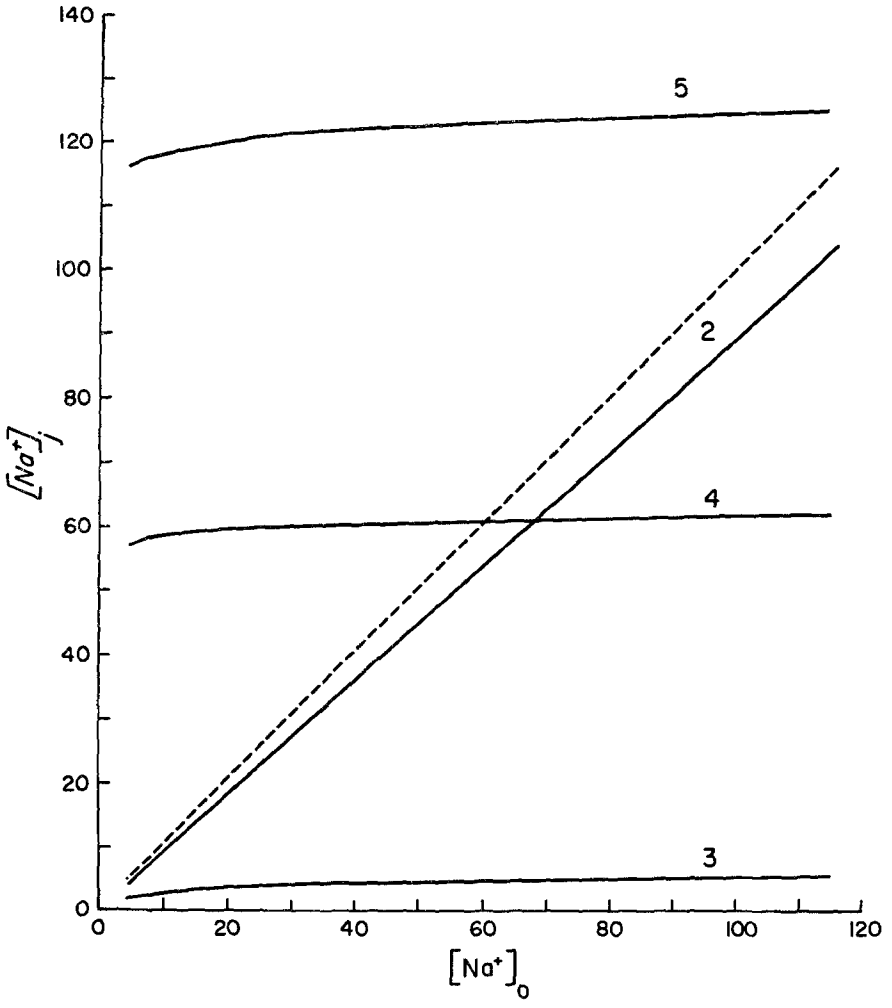

Fig. 4. Dependence of steady-state $[Na^+]$ in compartments 2, 3, 4, and 5 of the model membrane Fig. 1 shown in Fig. 1 of ref. [10], on $[Na^+]_0$

5.61 mM, respectively. If the border between compartments 2 and 3 is assumed to be Na^+ permselective, $V_{23} = 32.6$ mV for the lower $[Na^+]_1$, and 73.3 mV for the 10-times higher $[Na^+]_1$. Thus, there is an increase in V_{23} of 40.7 mV. Fig. 5 shows the results obtained on all models, and the linear regression line is also given. The 40-mV change per decade change in $[Na^+]_1$ agrees well with measurements on frog skin when changing $[Na^+]_0$ under a variety of solution conditions [2, 7, 15–17, 21]. The deviations of the computer data from the regression line are probably related to the fact that the k_{13} and k_{31} values were calculated with the help of curves shown in Fig. 1, which were drawn by eye (*see* Section 5*a*).

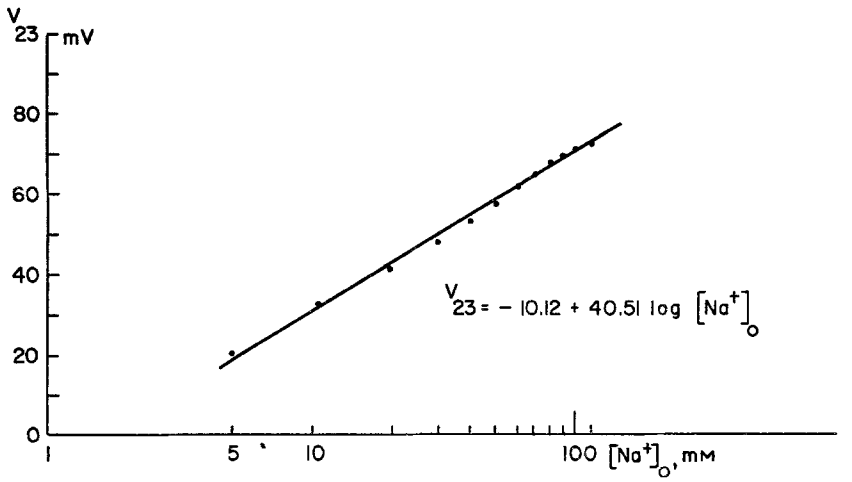

Fig. 5. Steady-state values for V_{23} when $[Na^+]_0$ increases from 5 to 115 mM. V_{23} is the electrical potential across the border between compartments 2 and 3 in the model membrane, assuming Na^+ permselectivity at this level, i.e., of the membrane between the subcorneal space and the 1. RCL

(e) Steady State Na^+ *Pool Fractions at Varying* $[Na^+]_1$ *(see also Section 4)*

For model 22, the following Na^+ pool values (S_j's, μEquiv) were read from the computer print-out data: During *influx* ($[Na^+]_1 = 5$ mM; $[Na^+]_7 = 0$), $S_{2i} = 0.0004514$; $S_{3i} = 0.0004057$; $S_{4i} = 0.0039880$; $S_{5i} = 0.0009994$. During *backflux* ($[Na^+]_1 = 0$; $[Na^+]_7 = 115$ mM), $S_{2b} = 0.0000145$; $S_{3b} = 0.0006420$; $S_{4b} = 0.22722$; $S_{5b} = 0.0573620$. During *net flux* ($[Na^+]_1 = 5$ mM; $[Na^+]_7 = 115$ mM), $S_{2n} = 0.0004658$; $S_{3n} = 0.0010477$; $S_{4n} = 0.23121$; $S_{5n} = 0.0583618$. In all cases $(S_{ji} + S_{jb}) = S_{jn}$. From these data, effective Na^+ pool fractions S_{ji}/S_{jn} were calculated. They were, during *influx:* $S_{2i}/S_{2n} = 96.89\%$; $S_{3i}/S_{3n} = 38.72\%$; $S_{4i}/S_{4n} = 1.72\%$; $S_{5i}/S_{5n} = 1.71\%$. During *backflux:* $S_{2b}/S_{2n} = 3.11\%$; $S_{3b}/S_{3n} = 61.28\%$; $S_{4b}/S_{4n} = 98.27\%$; $S_{5b}/S_{5n} = 98.29\%$. In practice, rates for influx and backflux are carried out by the use of isotopically labeled Na*. If such an "experiment" were done on model 22 membrane, thought to be in steady state with respect to "cold" Na^+ ($[Na^+]_1 = 5$ mM; $[Na^+]_7 = 115$ mM), and assuming that the specific activities of Na* (σ) in compartments 1 and 7 are equal ($\sigma_1 = \sigma_7 = 1.0$), the steady-state values for σ_2, σ_3, σ_4, and σ_5 during influx and backflux would be $f\sigma_1$ and $f'\sigma_7$, where f and f' are the percent values of the Na^+ pool fractions given above.

Similar calculations were carried out for all other models studied, varying $[Na^+]_1$ from 11.5 to 115 mM. We see no need to tabulate all results

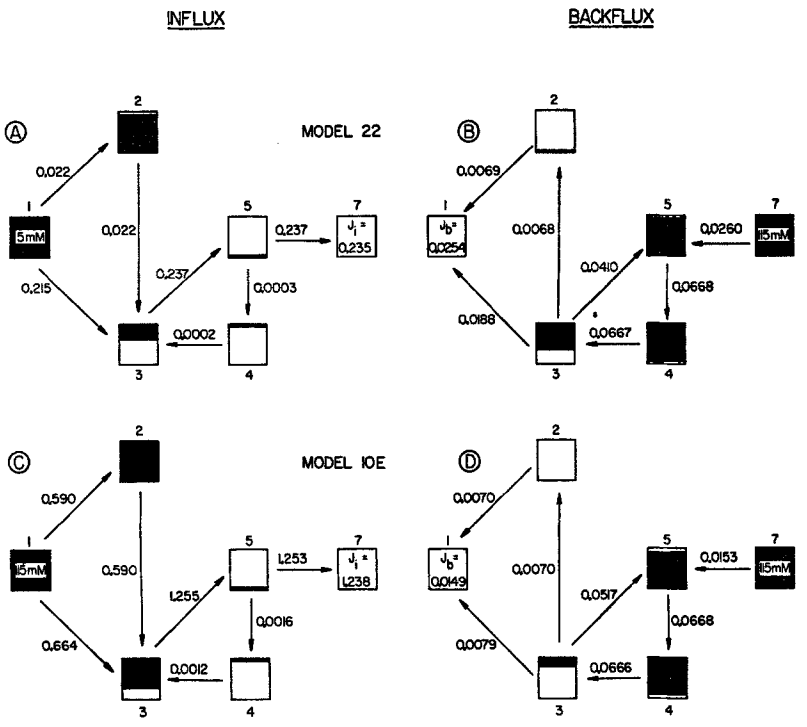

Fig. 6. Na^+ pool fractions (blackened areas) in compartments during steady state, models 22 and 10E. Figures at the arrows give net flux values in μEquiv × hr^{-1}. Foreward and backward fluxes at each level were as follows: *Model 22, influx:* $J_{12}=0.2389$; $J_{21}=0.2166$; $J_{13}=0.2269$; $J_{31}=0.0119$; $J_{23}=0.0271$; $J_{32}=0.0049$; $J_{34}=0.0010$; $J_{43}=0.0012$; $J_{35}=0.2434$; $J_{53}=0.0060$; $J_{45}=0.1196$; $J_{54}=0.1199$; $J_{57}=0.2398$; $J_{75}=0.0027$. *Backflux:* $J_{12}=0.0001$; $J_{21}=0.0070$; $J_{13}=0.0001$; $J_{31}=0.0189$; $J_{23}=0.0009$; $J_{32}=0.0077$; $J_{34}=0.0015$; $J_{43}=0.0682$; $J_{35}=0.3852$; $J_{53}=0.3442$; $J_{45}=6.8166$; $J_{54}=6.8834$; $J_{57}=13.7669$; $J_{75}=13.7929$. *Model 10E, influx:* $J_{12}=5.5139$; $J_{21}=4.9243$; $J_{13}=0.6892$; $J_{31}=0.0257$; $J_{23}=0.6155$; $J_{32}=0.0257$; $J_{34}=0.0051$; $J_{43}=0.0063$; $J_{35}=1.2862$; $J_{53}=0.0317$; $J_{45}=0.6319$; $J_{54}=0.6335$; $J_{57}=1.2671$; $J_{75}=0.0143$. *Backflux:* $J_{12}=0.00007$; $J_{21}=0.00710$; $J_{13}=0.00001$; $J_{31}=0.00792$; $J_{23}=0.00089$; $J_{32}=0.00792$; $J_{34}=0.00158$; $J_{43}=0.06822$; $J_{35}=0.39613$; $J_{53}=0.34444$; $J_{45}=6.82200$; $J_{54}=6.88884$; $J_{57}=13.77768$; $J_{75}=13.79297$

in detail; they are summarized in Figs. 6 and 7. The blackened areas in Fig. 6 give the size of the Na^+ pool fractions for models 22 and 10E. The top illustration in Fig. 7 gives values for total Na^+ pool fractions, calculated as $\Sigma S_{2i} S_{3i} S_{4i} S_{5i} / \Sigma S_{2n} S_{3n} S_{4n} S_{5n}$ (influx), and $\Sigma S_{2b} S_{3b} S_{4b} S_{5b} / \Sigma S_{2n} S_{3n} S_{4n} S_{5n}$ (backflux). Ordinates in the stippled areas give the percent pool fractions, at varying $[Na^+]_1$, during influx ($1 \rightarrow 7$); the difference between these values from 100% give the percent pool fractions during backflux ($7 \rightarrow 1$). At $[Na^+]_1 = 5$ mM ($[Na^+]_7 = 115$ mM, model 22) the total Na^+ pool fraction during influx is 2.0%, during backflux 98.0%. At $[Na^+]_1 =$

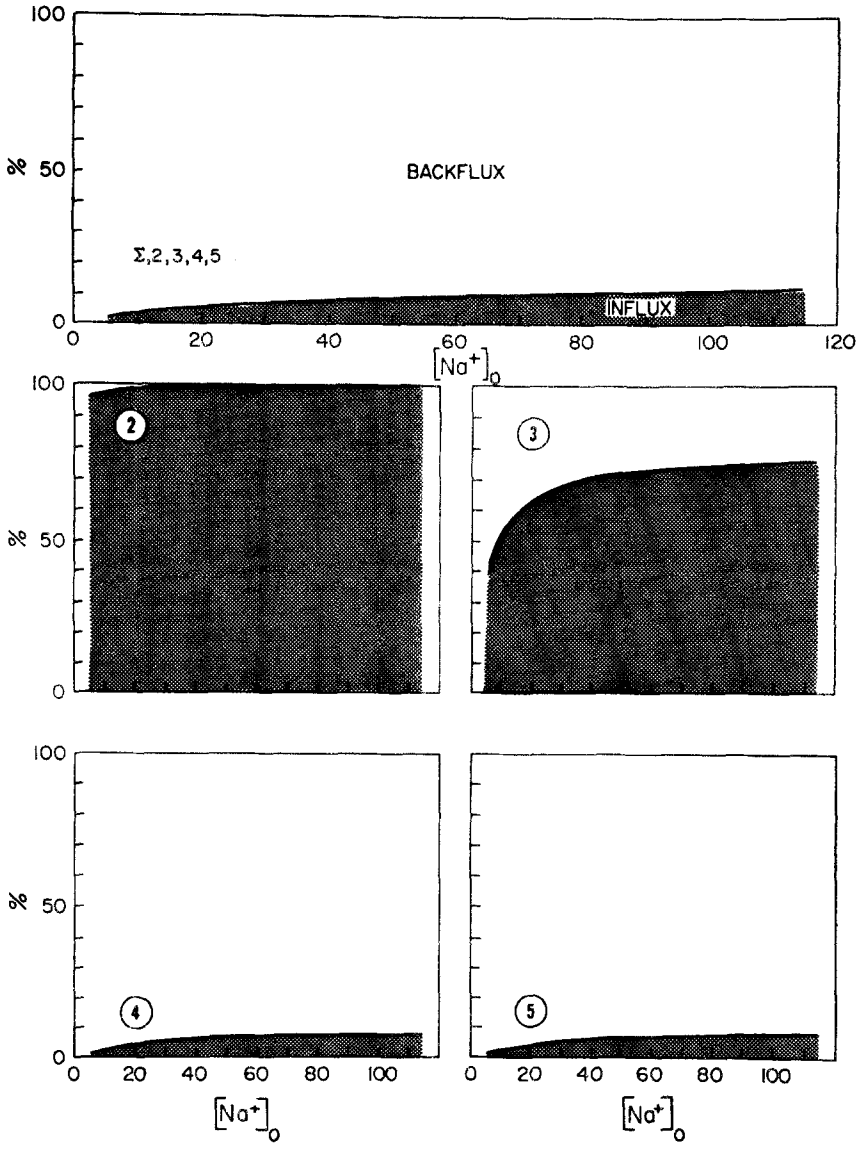

Fig. 7. Steady-state Na^+ pool fractions in individual compartments 2, 3, 4, and 5 as a function of $[Na^+]_0$ during influx and backflux conditions. Fractions are given as % of the Na^+ pool obtained during steady state under net flux conditions. Top of illustration: Total pool fraction calculated by adding individual steady-state Na^+ pools during influx (backflux) and dividing by total Na^+ pools during net flux

115 mM ($[Na^+]_7 = 115$ mM, model 10E) the corresponding values are 11.9%, and 88.1%, respectively. This agrees well with data on frog skin where it was found that only 10 to 12% of the skin can be labeled with Na* when applying Na* from the epidermal side [1, 4, 6, 18, 19].

(f) Intercompartmental Steady-State Na^+ *Fluxes at Varying* $[Na^+]_1$

From the steady state Na^+ pool sizes (S_j) and the assumed k values (Sections 1 and 2), inward and backward rates for fluxes of Na^+ between compartments were calculated for all models used. For example, $J_{12} = k_{12}S_1$, and $J_{21} = k_{21}S_2$. The difference between these flux values gave a value for net Na^+ flux between compartments. The numbers at the arrows in Fig. 6 give values for net flux of Na^+ between compartments in models 22 and 10E; i.e., for the lowest and the highest $[Na^+]_1$ considered in this study. The rates for inward and backward fluxes between compartments for the two models are given in the legend of Fig. 6. In all models a portion of the Na^+ entering the transmembrane Na^+ pump compartment 3, recycled between $3 \rightarrow 5 \rightarrow 4 \rightarrow 3$.

From Table 3e it can be seen that in both models, 22 and 10E, only about 0.1% of the Na^+ which entered the transport compartment 3 (via 1, 2, 4) under influx conditions recycles, and 99.9% comes directly and indirectly (via 2) from "outside" compartment 1. Under backflux conditions, about 61% (model 22) and 78% (model 10E) of the Na^+ entering the transport compartment 3 is recovered from loss towards the outside by recycle; 39% and 22%, respectively, are lost towards the outside. Finally,

Table 3. Steady-state rates of Na^+ recycling between compartments $3 \rightarrow 5 \rightarrow 4 \rightarrow 3$, and transmembrane Na^+ flux rates

	Model 22	Model 10E
	$\mu Equiv \times cm^{-2} \times hr^{-1}$	$\mu Equiv \times cm^{-2} \times hr^{-1}$
(a) Transmembrane influx (J_i^{Na})	0.237	1.254
(b) Transmembrane backflux (J_b^{Na})	0.026	0.015
(c) Transmembrane net flux (J_n^{Na})	0.211	1.239
(d) Net rate of Na^+ entry into 3 [a]	$\mu Equiv \times hr^{-1}$	$\mu Equiv \times hr^{-1}$
Influx condition [b]	0.2372	1.2552
Backflux condition [c]	0.0667	0.0666
Net flux condition [d]	0.2785	1.3061
(e) Net rate of Na^+ recycling	in % of values given under (d)	
Influx condition	0.08	0.10
Backflux condition	61.47	77.63
Net flux condition	24.01	5.19

[a] In influx from compartments 1, 2 and 4. In backflux from compartment 4.
[b] *Model 22:* $[Na^+]_1 = 5$ mM; $[Na^+]_7 = 0$ mM. *Model 10*E: $[Na^+]_1 = 115$ mM; $[Na^+]_7 = 0$ mM.
[c] *Models 22 and 10*E: $[Na^+]_1 = 0$ mM; $[Na^+]_7 = 115$ mM.
[d] Data not illustrated as those in Fig. 6. *Model 22:* $[Na^+]_1 = 5$ mM; $[Na^+]_7 = 115$ mM. *Model 10*E: $[Na^+]_1 = 115$ mM; $[Na^+]_7 = 115$ mM.

under net flux conditions, with Na^+ moving from $1 \rightarrow 7$, 24% of the Na^+ entering 3 recycles, and 76% comes from the outside in model 22. In model 10E the corresponding figures are: 5% of the Na^+ recycles, and 95% entering 3 comes from the outside.

6. Discussion

In the preceding paper [10] we have pointed out that in model 10E the needed rate coefficients were chosen in such proportion to each other that the function of the model was in agreement with several laboratory observations made on frog skin. In a system with as many as 14 unknown rate coefficients, it should always be possible to achieve simulation of laboratory data by changing several or all variables simultaneously, but the result thus obtained would be of little or no interest. On the other hand, if a change in only one of the seven pairs of rate coefficients selected for model 10E should lead to results which are in good agreement with laboratory facts, the conceptual and heuristic aspects of this model, we believe, merit attention. It is with this in mind that we have challenged the operation of model 10E.

(a) Transmembrane Flux Rates, and V_{23} at Varying $[Na^+]_1$

The experimental data on frog skin (*see* Sections 5*b* and 5*d*) show that Na^+ influx and net flux, and, to a lesser degree Na^+ backflux, increase with increasing $[Na^+]_0$ until at $[Na^+]_0 \cong 115$ mM a certain maximal flux value is obtained. For skins of the European frog species, and *Rana pipiens*, the maximal net flux value is approximately 1 $\mu Equiv \times cm^{-2} \times hr^{-1}$. The skin potential increases, mostly, by approximately 35 mV for a 10-fold increase in $[Na^+]_0$. The results obtained with the model 10E simulate these results very closely, if one lets the parameters k_{13} and k_{31} change with $[Na^+]_1$ in the manner as has been experimentally established by the work of Cereijido *et al.* [3]. These authors have obtained values for the rate constants at the site of entry of Na^+ by assuming a three-compartment model in which the epidermis is treated as the middle compartment, located between outside and inside fluid compartments. As mentioned in Section 5*a*, we have used their data in a somewhat biased fashion in that we have let only k_{13} and k_{31} change with $[Na^+]_1$, but kept k_{12}, k_{21} (and all other k's) as in 10E. At this time we can justify this by pointing out that only then, and not by also changing k_{12} and k_{21}, model 10E behaved as does skin epidermis, both in regard to flux and p.d. changes. This coincidence suggests

that perhaps in frog skin the pathway $1 \leftrightarrow 3$ is more affected by changing $[Na^+]_0$ than in pathway $1 \leftrightarrow 2$. Pathway $1 \leftrightarrow 3$ is from: outside solution $\leftrightarrow$ cornified layer/cell junctions $\leftrightarrow$ cell fluid of the 1. RCL. Pathway $1 \leftrightarrow 2$ is from: outside solution $\leftrightarrow$ cornified layer $\leftrightarrow$ fluid in the subcorneal space. There is, then, a greater structural asymmetry involved in pathway $1 \leftrightarrow 3$ than in pathway $1 \leftrightarrow 2$. Schultz [20] has pointed out that passive asymmetrical fluxes may be seen in cases of flow of material across membranes of structural heterogeneity. Simple Fickean diffusion alone does not describe the forward and reversed flux kinetics, and this is the way frog skin seems to behave at the level of entry of Na^+ into the skin [3]. By the same reasoning, for the present, no influence of a structural asymmetry at the level between compartments 2 and 3 has been considered, although this needs to be investigated.

In regard to the use of Eqs. (4) and (8) to describe the dependence of net Na^+ flux across the skin and the model membrane, it should be said that both equations lack adequate theoretical and factual support to make their use inevitable. They are, however, useful empirical models for presentation of results in a quantitative manner.

(b) Transmembrane Backflux at Varying $[Na^+]_1$

The results given in Table 2 show that the rate of Na^+ backflux decreases with increasing $[Na^+]_1$. This is in apparent disagreement with laboratory studies on electrically open-circuited [22], or short-circuited [13] frog skin. In either case it has been found that backflux (outflux) increased with increasing $[Na^+]_0$. There are, presently, very few experimental data available to resolve this issue. A possible explanation, however, is the following one: Ussing [22] has pointed out that during the first hour after changing from $[Na^+]_0 = 115$ mM to 1 mM, Na^+ outflux remains high. Only after a considerable lag period of 1 to 2 hr a decrease in backflux is observed. He suggests that this may be a biologically useful adaptation reaction, with permeability change in skin. To model this feature, i.e., adaptability of the skin to low $[Na^+]_0$ leading to flux changes, certain k coefficients in model 10E would have to be altered with respect to time.

(c) $[Na^+]$ *and* Na^+ *Pool Fractions at Varying* $[Na^+]_1$

By varying $[Na^+]_1$ from 5 to 115 mM, $[Na^+]_2$ (subcorneal space) in steady-state conditions was always less than $[Na^+]_1$. The difference $[Na^+]_2 - [Na^+]_1$ increased with increasing $[Na^+]_1$ (Fig. 4). It may be

possible to test this prediction by puncturing the subcorneal space in skin epidermis. $[Na^+]_3$ also was found to be less than $[Na^+]_1$ at all $[Na^+]_1$ values tested. This means that in all cases Na^+ entered the system in the direction of a falling $[Na^+]$ gradient. We do not wish to imply that in skin electrical potentials are not also involved in the movement of Na^+, but for the present, these forces are not reflected separately from the chemical potentials in the assumed k (or the associated apparent permeability) coefficients in model 10E. Studies along these lines are a challenge for the future. We do not see insurmountable difficulties in such modelling work. Here, as in the case of adaptability (*see above*), the question is whether there are sufficient electrical data available to be applied to the multicompartmental model 10E.

Model 10E is in agreement with observations on skin, in that only about 12% of the total Na^+ in the epidermal system could be labeled with Na* at $[Na^+]_1 = [Na^+]_7 = 115$ mM. For the case $[Na^+]_1 = 5$ mM and $[Na^+]_7 = 115$ mM this labeling fraction was 2%. This prediction could be tested on skin.

Appendix

Computational Error Analysis

(1) A preliminary check on the numerical accuracy of the CSMP calculated numerical solutions to the differential equations of model 10E revealed that the differential equations [10] were not satisfied to a high enough degree of accuracy. The inaccuracy seemed to be mostly in compartment 1, where a relatively large initial condition was used. We first thought that this was due to the inaccuracies of using very small numbers in the variable step size Runge-Kutta numerical integration scheme. When changes in the minimum integration interval failed to alleviate the problem, we decided to multiply the derivatives of the functions by an appropriate constant just before the numerical integration, then divide by this same constant immediately after the numerical integration, a procedure suggested to us by H.P.T. Corley, Department of Biometry. The constants used were: 100 (for compartment 5), 1,000 (for compartments 2, 3 and 4), and 10,000 for compartments 1 and 7.

This procedure yielded solutions which satisfied the differential equations quite well. As a check we used the number 1.0 for all compartments, rather than the factors given above, and obtained results almost as good as when the much larger numbers were used. At this point we felt the need for an independent check of the accuracy of our computations. We proceeded as follows.

The differential equations we used can be written in matrix from as follows:

$$\dot{x}=Kx$$

with solution [12]

$$x=\exp(Kt)\,x_0$$

where x_0 is the vector of initial conditions and K is the matrix of rate coefficients k. We programmed directly in Fortran, double precision:

$$\exp(Kt)=\left(I+Kt+\frac{K^2t^2}{2!}+\cdots\right)$$

where I is the identity matrix, and found that these calculated solutions agreed "exactly" with the solutions using the constant multipliers above. This approach required much less computer time than the CSMP runs and may, therefore, be an alternative to CSMP for these types of differential equations. Unfortunately, we do not have a satisfactory explanation at this time of the fact that factors of one were almost as good in CSMP as were factors of powers of ten.

(2) A comparison of Fig. 6*D* with Fig. 3 (lower right) of the preceding paper [10] reveals a discrepancy in the data for net flux out of compartment 7, and into compartment 1. Here, as in model 12G [10], we were led to attribute this to the fact (page 58 of the preceding paper) that compartment 5 was not quite near steady state. From the data shown in Fig. 6*D* (where a much smaller discrepancy still exists) we must now conclude that the main reason for the discrepancy noted in Fig. 3 of the previous paper is attributable to greater computational errors, which we have now overcome, as explained above.

This work was supported by NIH Grants GM-03545-19 and 5K06GM 16,687-10.

References

1. Aceves, J., Erlij, D. 1971. Sodium transport across the isolated epithelium of the frog skin. *J. Physiol.* **212**:195
2. Cereijido, M., Curran, P. F. 1965. Intracellular electrical potentials in frog skin. *J. Gen. Physiol.* **48**:543
3. Cereijido, M., Herrera, F. C., Flanigan, W. J., Curran, P. F. 1964. The influence of Na concentration on Na transport across frog skin. *J. Gen. Physiol.* **47**:879
4. Cereijido, M., Reisin, I., Rotunno, C. A. 1968. The effect of sodium concentration on the content and distribution of sodium in the frog skin. *J. Physiol.* **196**:237
5. Curran, F. P., Herrera, F. C., Flanigan, W. J. 1963. The effect of Ca and antidiuretic hormone on Na transport across frog skin. *J. Gen. Physiol.* **46**:1011

6. Dörge, A., Nagel, W. 1970. Effect of amiloride on sodium transport in frog skin. II. Sodium transport pool and unidirectional fluxes. *Pflüg. Arch. Ges. Physiol.* **321**:91
7. Greven, K. 1941. Ein Beitrag zum Problem des Ruhestroms der Froschhaut. *Pflüg. Arch. Ges. Physiol.* **244**:365
8. Hoshiko, T. 1961. Electrogenesis in frog skin. *In:* Biophysics of Physiological and Pharmacological Actions. p. 31. American Association for the Advancement of Science, Washington, D.C.
9. Huf, E. G. 1936. Über aktiven Wasser- und Salztransport durch die Froschhaut. *Pflüg. Arch. Ges. Physiol.* **237**:143
10. Huf, E. G., Howell, J. R. 1974. Computer simulation of sodium fluxes in frog skin epidermis. *J. Membrane Biol.* **15**:47
11. Huf, E. G., Wills, J. P., Arrighi, M. F. 1955. Electrolyte distribution and active salt uptake in frog skin. *J. Gen. Physiol.* **38**:867
12. Jacquez, J. A. 1972. Compartmental Analysis in Biology and Medicine. Elsevier Publishing Company, Amsterdam
13. Kirschner, L. B. 1959. The interaction between sodium outflux and the sodium transport system in the frog skin. *J. Cell. Comp. Physiol.* **53**:85
14. Koefoed-Johnson, V., Ussing, H. H. 1958. The nature of the frog skin potential. *Acta Physiol. Scand.* **42**:298
15. Linderholm, H. 1952. Active transport of ions through frog skin with special reference to the action of certain diuretics. *Acta Physiol. Scand.* **27** (Suppl. 97):1
16. Linderholm, H. 1954. On the behavior of the "sodium pump" in frog skin at various concentrations of Na ions in the solution on the epithelial side. *Acta Physiol. Scand.* **31**:36
17. Lindley, B. D., Hoshiko, T. 1964. The effects of alkali metal cations and common anions on the frog skin potential. *J. Gen. Physiol.* **47**:749
18. Nagel, W., Dörge, A. 1970. Effect of amiloride on sodium transport of frog skin. I. Action on intracellular sodium content. *Pflüg. Arch. Ges. Physiol.* **317**:84
19. Nagel, W., Dörge, A. 1971. A study of the different sodium compartments and the transepithelial sodium fluxes of the frog skin with use of ouabain. *Pflüg. Arch. Ges. Physiol.* **324**:267
20. Schultz, J. S. 1971. Passive asymmetric transport through biological membranes. *Biophys. J.* **11**:924
21. Smith, T. C., Martin, J. H., Huf, E. G. 1973. Na^+ pool and Na^+ concentration in epidermis of frog skin. *Biochim. Biophys. Acta* **291**:465
22. Ussing, H. H. 1949. The active ion transport through the isolated frog skin in the light of tracer studies. *Acta Physiol. Scand.* **17**:1
23. Ussing, H. H., Zerahn, K. 1951. Active transport of sodium as the source of electric current in the short-circuited isolated frog skin. *Acta Physiol. Scand.* **23**:110